Step-Size Is Determined by Neck Length in Myosin V†

Takeshi Sakamoto,‡ Ahmet Yildiz,§ Paul R. Selvin,§ and James R. Sellers*,‡

Laboratory of Molecular Physiology, National Heart, Lung and Blood Institute, National Institutes of Health, Bethesda, Maryland 20892-1762, and the Department of Physics and Center for Biophysics and Computational Biology, University of Illinois at Urbana-Champaign, Urbana, Illinois 61801

Received June 23, 2005; Revised Manuscript Received August 26, 2005

ABSTRACT: The highly processive motor, myosin V, has an extremely long neck containing six calmodulin-binding IQ motifs that allows it to take multiple 36 nm steps corresponding to the pseudo-repeat of actin. To further investigate how myosin V moves processively on actin filaments, we altered the length of the neck by adding or deleting IQ motifs in myosin constructs lacking the globular tail domain. These myosin V IQ mutants were fluorescently labeled by exchange of a single Cy3-labeled calmodulin into the neck region of one head. We measured the step-size of these individual IQ mutants with nanometer precision and subsecond resolution using FIONA. The step-size was proportional to neck length for constructs containing 2, 4, 6, and 8 IQ motifs, providing strong support for the swinging lever-arm model of myosin motility. In addition, the kinetics of stepping provided additional support for the hand-over-hand model whereby the two heads alternately assume the leading position. Interestingly, the 8IQ myosin V mutant gave a broad distribution of step-sizes with multiple peaks, suggesting that this mutant has many choices of binding sites on an actin filament. These data demonstrate that the step-size of myosin V is affected by the length of its neck and is not solely determined by the pseudo-repeat of the actin filament.

Using biochemical assays, myosin V has been thoroughly characterized as a high duty ratio motor (*1*−*3*), spending a large fraction of its total enzymatic cycle time strongly bound to the actin filament. This kinetic property, along with the myosin V's unique long neck structure as a dimeric molecule, allows it to be highly processive. Therefore, the motor may undergo multiple enzymatic cycles while at least one head of the molecule is attached to the actin filament at anytime. This adaptation aids in the specific biological function of myosin V as a long-range vesicle transporter in cells (*4*, *5*).

The mouse myosin V heavy chain consists of an amino terminal motor domain joined to a long "neck" region containing six IQ motifs specific for calmodulin (CaM)[1] binding, followed by a carboxyl-terminal coiled-coil region and globular tail (*6*). The long neck region, which most likely functions as a lever-arm to amplify small nucleotide-dependent structural changes in the motor domain, permits myosin V to take steps of an average distance of ∼36 nm, coinciding with the length of the half-pitch of an actin filament (*2*, *7*). This step consists of a working stroke (defined as the distance myosin V translocates actin in a single movement of the lever-arm), followed by a diffusive search by the new lead head for a suitable binding site on actin. In studies with myosin II or myosin V mutants with different numbers of IQ motifs, the average working stroke taken by myosin in single interactions with actin was found to be proportional to neck length (*8*−*13*). In addition, one of these studies showed that the step-size of myosin V during processive runs in an optical trap was shorter for a construct containing four IQ motifs than in a native six IQ motif construct. However, another study using a chimeric myosin V, consisting of the motor domain and the first IQ motif of myosin V which were fused to the rod of smooth muscle myosin, was shown to generate a large (36 nm) step (*14*). This latter study raised the question of whether the step-size of myosin V is determined by the neck length or by the pseudo-repeat of the actin filament. While the working stroke of myosin V during single interactions with actin has been characterized using a variety of myosin V constructs with shorter and longer neck length mutants, the step-size during processive runs has not.

Here, in this study, fluorescently labeled calmodulins were exchanged into recombinant myosin V HMM (heavy meromyosin)-like mutants with shorter (2IQ-HMM and 4IQ-HMM) and longer (8IQ-HMM) neck lengths. The stepping motion of mutant and wild-type myosin V molecules on actin were observed using FIONA (*F*luorescent *I*maging with *O*ne *N*anometer *A*ccuracy) (*15*), which allows for nanometer precision in the localization of myosin during processive runs under unloaded conditions. Analysis of the stepping distribution demonstrated that the step-size of different neck length mutants of myosin V also is proportional to increasing neck length. These results are consistent with the hand-over-hand lever-arm model of actomyosin mechanics. Furthermore, the

† This work was supported by a fellowship from the Japanese Society for the Promotion of Science Research Fellowships for Japanese Biomedical and Behavioral Researchers at NIH to T.S. and by NHLBI intramural funds.

* Corresponding author: James R. Sellers, Laboratory of Molecular Physiology, National Heart, Lung and Blood Institute, National Institutes of Health, Building 10, Room 8N202, Bethesda, MD 20892-1762. Tel: 301-496-6887. Fax: 301-402-1542. E-mail: sellersj@nhlbi.nih.gov.

‡ National Institutes of Health.

§ University of Illinois at Urbana-Champaign.

[1] Abbreviations: HMM, heavy meromyosin; TIRF, total internal reflection fluorescence; FIONA, fluorescence imaging with one nanometer accuracy; CaM, calmodulin; PSF, point spread function.

10.1021/bi0512086 CCC: $30.25
Published on Web 11/16/2005

step-size distribution for the 8IQ-HMM construct was broad and showed multiple peaks, suggesting that this molecule may bind to one of several actin monomer targets, including the azimuthally preferred actin located 36 nm away from the attached head. Thus, the neck length and possibly the stiffness of these myosin V mutants may contribute significantly to the stepping mechanics of these highly processive motors.

EXPERIMENTAL PROCEDURES

Preparation of Proteins. Rabbit skeletal muscle actin (*16*) was prepared as previously described, (*3*). Actin filaments were prepared by mixing biotinylated actin and unlabeled actin in a 1:10 ratio, respectively, followed by incubation with phalloidin. Construction methods of the IQ mutants were described elsewhere (*8*). Briefly, all molecules contained the motor domain and the coiled-coil region terminating at the position equivalent to residue 1091 of HMM-6IQ followed by a FLAG tag. 2IQ-HMM contained IQ motifs 1 and 6; 4IQ-HMM contained motifs 1, 2, 5, and 6; 6IQ-HMM contained motifs 1, 2, 3, 4, 5, and 6; 8IQ-HMM contained motifs 1, 2, 3, 4, 3, 4, 5, and 6. In all these cases, the IQ motifs appeared in the order given, and care was taken to preserve the 23/25 amino acid repeat between IQ motifs (*8*). 2Ala6IQ-HMM contain motifs 1, 2, 3, 4, 5, and 6 with two alanine residues inserted between motifs 3 and 4 to disrupt this repeat without significantly changing the length. The exchange of a single Cy3-labeled calmodulin (CaM) into the IQ-HMM mutants was carried out as previously described using a 1:20 Cy3-CaM/myosin V ratio (*3*, *17*). In some experiments, a 1:1 ratio was used.

Single Molecule in Vitro Motility Assay. FIONA (*F*luorescence *I*maging with *O*ne *N*anometer *A*ccuracy), a single molecule motility assay using TIRF microscopy, was performed and quantified as described previously (*15*). Motility buffer used for the assay was as follows: 20 mM MOPS (pH 7.4), 5 mM $MgCl_2$, 0.1 mM EGTA, 50 mM KCl, 0.3 μM ATP, 1 μM CaM, and 50 mM dithiothreitol, at 23 °C. An oxygen scavenging system modified for use with FIONA (*15*) was also added to the motility buffer.

Data Analysis. Data acquisition and analysis were performed as described previously (*15*). Step-size histograms were fit to single and sum of Gaussians. Dwell time histograms of the HMM-IQ mutants were curve-fitted to the kinetic hand-over-hand model (*15*) using the following equation: $P(t) = tk^2 \exp(-kt)$.

The fluorescence intensities of individual spots were determined by measuring the intensity of a 10 × 10 pixels area surrounding each fluorescent spot, followed by subtraction of a nearby "background" area of the same size where no strong fluorescence was observed. The distributions of fluorescence intensity of both small and large steppers were then normalized with respect to the measured intensity of a single Cy3-labeled CaM.

RESULTS

Labeling Ratio between Cy3-CaM and IQ Mutants. To examine the role of the neck region of myosin V in determining step-size, IQ motifs were either added or subtracted to create mutant myosin V HMM molecules with either longer or shorter neck regions. These molecules will be referred to as *n*IQ-HMM where n = the number of IQ motifs present per heavy chain. An additional mutant, termed 2Ala6IQ-HMM, was created by insertion of two alanine residues between the third and fourth IQ motifs of a 6IQ-HMM. This mutation does not effectively increase the length of the neck, but may increase the flexibility by disrupting normal interactions between the third and fourth CaMs. To visualize myosin V molecules using total internal reflection fluorescence (TIRF) microscopy, Cy3-labeled CaM (Cy3-CaM) was exchanged for endogenous CaM molecules under conditions where, ideally, only one CaM per myosin V molecule was replaced. We used two methods to determine the number of Cy3-CaM molecules exchanged per myosin V, as described previously (*3*, *8*). First, the concentration of the HMM-IQ mutant and the number of moles of Cy3 incorporated into CaM were measured in solution using the appropriate extinction coefficients after repurification of the exchanged protein. By this criteria, only about 1 in every 5−10 myosin V HMM molecules received a Cy3-CaM. Second, we observed the photobleaching kinetics of single spots of HMM-IQ mutants bound to cover slips using TIRF microscopy. The percentages of single photobleaching events of all HMM-IQ mutants were between 82 and 95% when exchanged under these conditions. Note that the labeling ratio of Cy3/CaM is 0.7. Thus, most of the myosin V molecules contain a single Cy3-CaM.

Measurement of Step-Size of HMM-IQ Mutants. The movements of these single fluorescently labeled HMM-IQ molecules on actin bound to a coverslip surface were visualized by TIRF microscopy. The FIONA method, whereby the point spread function (PSF) was fitted by a two-dimensional (2-D) Gaussian, was used to determine the localization of the labeled myosin head. This method has been shown to achieve about 1.5 nm localization (*15*). The fluorescent spots moved in distinct steps as a function of time at 0.3 μM ATP (Figure 1). This low ATP concentration was used to slow the stepping rate sufficiently so that 0.5 s time acquisitions could be taken to accumulate sufficient photons to allow for the Gaussian fitting. Note the different values of the displacement axes in Figure 1. It can be seen that the step-size increases with neck length. Occasionally, traces were found for a particular HMM-IQ mutant that gave steps of about one-half the size (called "small steppers") of those found in the majority of traces for that mutant. We will show evidence below that these small stepper traces arise from molecules in which both heads contain an exchanged Cy3-CaM.

The relationship between step-size and neck length is more clearly demonstrated in histograms (Figure 2). Step-sizes of the 2IQ-, 4IQ-, and 6IQ-HMM mutants obtained from fitting the distributions were 22.9 ± 6.4, 50.2 ± 9.9, and 75.3 ± 9.0 nm, respectively. Note that these values represent the distance that a labeled head travels when moving from the trailing to leading position. The step-size measured by FIONA will thus be twice the value obtained in optical trapping experiments where the center of mass movement of the molecule is followed. It can also be seen in this figure that the step-sizes of the "small steppers" (black bars) for 2IQ-, 4IQ-, and 6IQ-mutants (11.3 ± 2.3, 28.6 ± 9.0, and 35.2 ± 8.0 nm, respectively) were about one-half the length of the majority of the molecules.

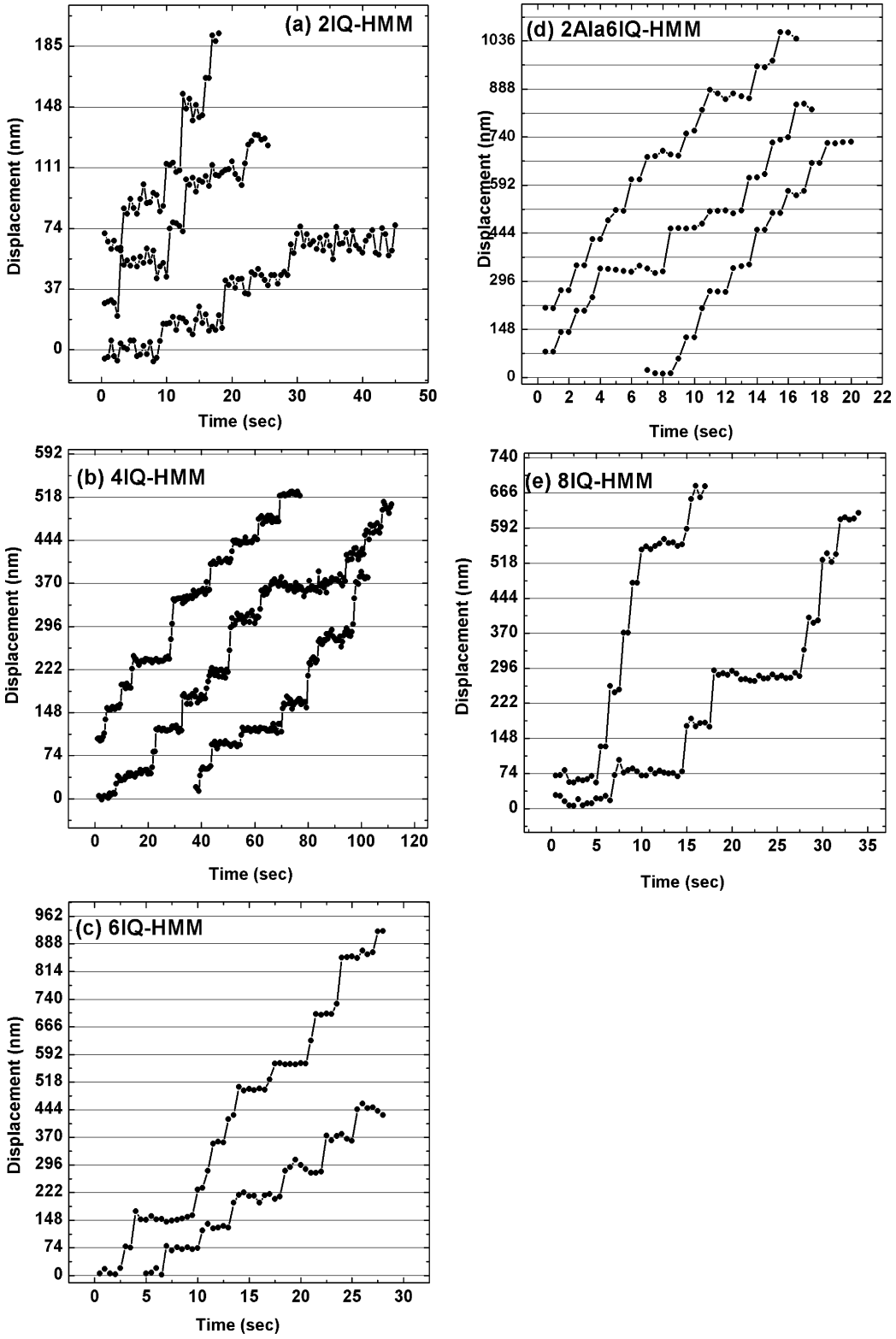

FIGURE 1: Stepping traces of HMM-IQ mutants measured by FIONA. (a) 2IQ-HMM, (b) 4IQ-HMM, (c) 6IQ-HMM, (d) 8IQ-HMM, and (e) 2Ala6IQ-HMM. Each data point represents a 0.5 s acquisition time. Note the different scales.

The individual traces for the 2Ala6IQ-HMM mutant could not be easily sorted into small and large steppers, so all the data were plotted together for this mutant. Instead, all traces showed that 2Ala6IQ-HMM takes irregularly spaced steps between 32 and 85 nm in length (Figures 1d and 2d). Although the histogram was well-fitted by a single Gaussian function, the standard deviation (±20.3 nm) was considerably larger than that of wild-type HMM or short neck length molecules. The overall step-size of this mutant (67.5 nm) was fairly similar to that of 6IQ-HMM. The 8IQ-HMM mutant traces were also resolved into mostly "large steppers" (Figure 2e) with some "small steppers" (data not shown). This mutant showed a much broader and multimodal distribution of step-sizes. The average step-size of the events shown in Figure 2e was 96 ± 18.3 nm. The data clearly could not be fitted by a single Gaussian function. Fitting all

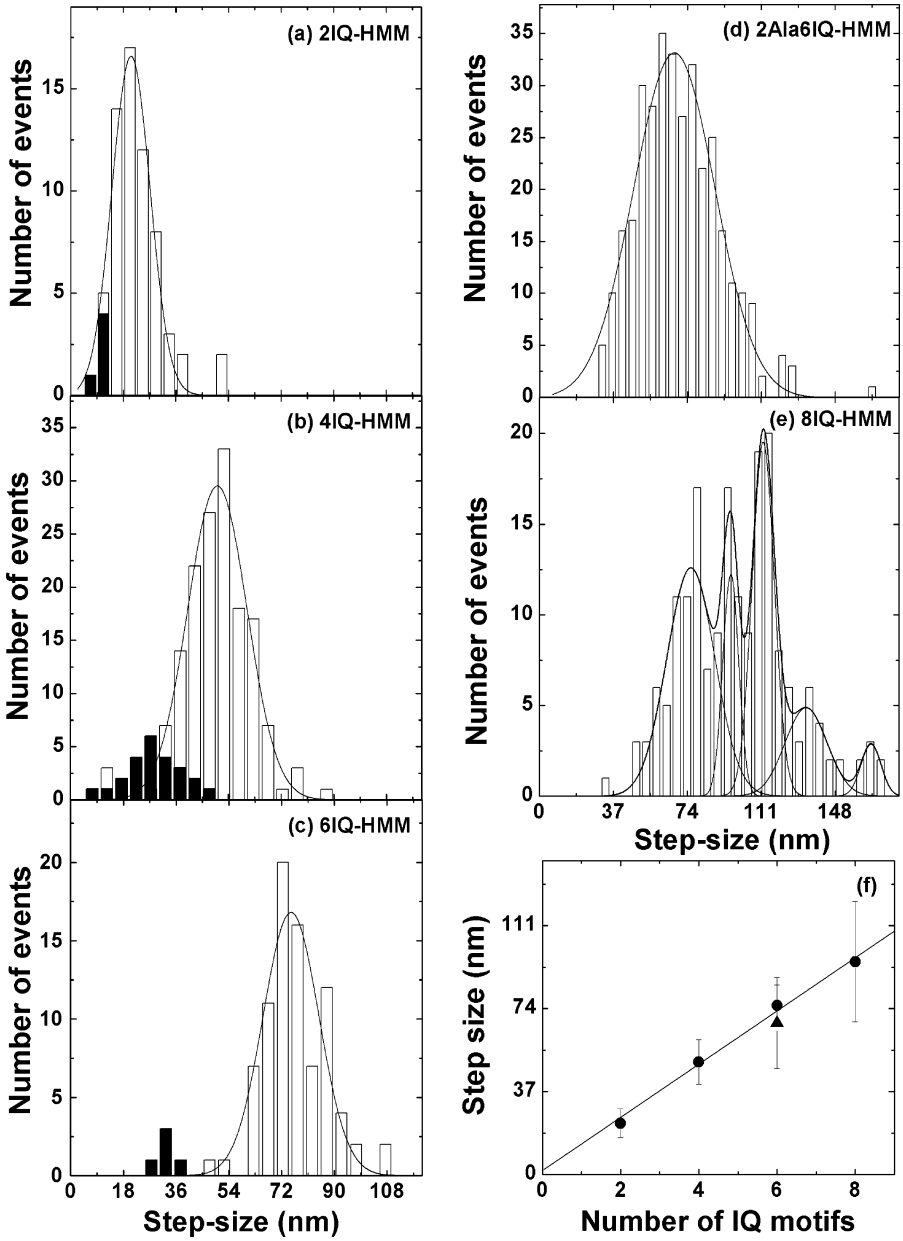

FIGURE 2: Histogram of step-sizes of IQ mutants. Bars show distribution of step-size for large (white bars) and small steppers (black bars). (a) 2IQ-HMM, (b) 4IQ-HMM, (c) 6IQ-HMM, (d) 2Ala6IQ-HMM, and (e) 8IQ-HMM. The solid black line in panels a−d are fits of the large steppers (white bars) to a single Gaussian curve. The solid black line in panel e is a fit to a sum of five Gaussian distributions using the maximal likelihood method (*23*). The multimodal fit was justified by the AC scoring method (*24*, *25*). The value for this fit was $p < 0.04$. Small steppers data are not shown with 8IQ-HMM in panel e. The peaks of large step-size of HMM-IQ mutants (mean ± SD) are 22.9 ± 6.4 nm (2IQ-HMM, $n = 58$, $\chi^2 = 0.99$, $r^2 = 0.97$), 50.2 ± 9.9 nm (4IQ-HMM, $n = 154$, $\chi^2 = 2.07$, $r^2 = 0.98$), 75.3 ± 9.3 nm (6IQ-HMM, $n = 83$, $\chi^2 = 2.98$, $r^2 = 0.94$), and 67.5 ± 20.3 nm (2Ala6IQ-HMM, $n = 336$, $\chi^2 = 2.04$, $r^2 = 0.96$). The 8IQ-HMM step-size distribution has five peaks (total $n = 191$, $\chi^2 = 2.24$, $r^2 = 0.96$) 75.8 ± 11.9, 95.8 ± 6.7, 112.1 ± 5.1, 133.5 ± 10.3, and 165.0 ± 5.2 nm. The peaks of small steppers for the HMM-IQ mutants are 11.1 ± 2.3 nm (2IQ-HMM, $n = 5$), 28.6 ± 9.0 nm (4IQ-HMM, $n = 23$), 35.2 ± 8.0 nm (6IQ-HMM, $n = 5$), and 51.8 ± 13.8 nm (8IQ-HMM, $n = 47$) (data not shown for clarity). The small and large stepping traces could not be separated in the case of the 2Ala6IQ-HMM mutant. (f) Plot of step-size vs the number of IQ motifs. Black triangle is 2Ala6IQ-HMM.

the data reveals five peaks at 75.8 ± 11.9, 95.8 ± 6.7, 112.1 ± 5.1, 133.5 ± 10.3, and 165 ± 5.2 nm. The two minor peaks with the largest step-sizes may represent cases in which rapid smaller steps occurred without a discernible intervening plateau phase.

A plot of the average step-size versus the number of IQ motifs is linear (Figure 2f).

Small Steppers Have Labels on Both Heads. As stated above, occasionally, processive runs having step-sizes that were about one-half the length of the majority of the runs for a given mutant were seen. Three lines of evidence suggest that these small steppers represent molecules where both heads contain an exchanged Cy3-CaM. These molecules were imaged as a single fluorescent spot since the two fluorophors are within the Rayleigh diffraction limit. Thus, the movement of the center of mass of two dyes would be observed at each step. First, the percentage of these small stepper traces dramatically increases when higher Cy3-CaM concentrations were used for exchange (data not show). Second, the fluorescent intensities of small stepper spots were

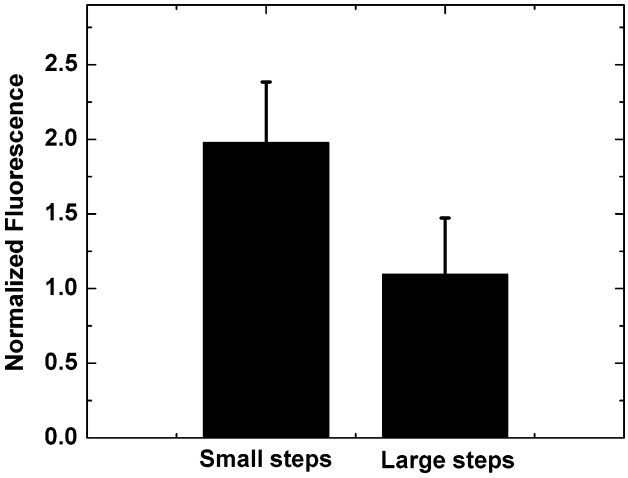

FIGURE 3: Normalized fluorescence intensity of individual spots from small and large stepper traces for the 6IQ-HMM mutant. See Experimental Procedures for details.

approximately twice that of large steppers (Figure 3). Third, analysis of the dwell times, the time between steps, also supports this contention (*15*). For a myosin with only one labeled head and where the label is near the motor domain (i.e., first IQ position), only the movement of the labeled head is observed; the alternating movement of the unlabeled head is silent. Yildiz et al. (*15*) showed that a plot of the dwell time distribution, $P(t)$, for such a case is characterized by an initial rise and then a decline since the derived kinetic equation for this type of movement is $P(t) = tk^2\ e^{-kt}$, assuming the stepping rates (k) of the two heads are equal. This was indeed seen when the dwell times of the large steppers were plotted (Figure 4). In contrast, if both heads contain a labeled Cy3-CaM near the motor domain, the movement of both heads would be observed, and the dwell time reduces to a single exponential, $P(t) = k\ e^{-kt}$. We find that the dwell time distribution for small steppers of 4IQ-HMM was fit by a single exponential and that its rate (0.47 s^{-1}) is almost twice as fast as that of 4IQ-HMM large steppers (0.28 s^{-1}).

DISCUSSION

Previous work has shown that under loaded conditions in optical traps the working stroke of myosin V neck mutants is a function of the length of the lever-arm (*8*−*10*). Here, we used the FIONA modification of the single molecule TIRF motility assay to follow the fluorescently labeled myosin V mutants as they moved processively along actin filaments with nanometer precision under unloaded conditions. There was a linear correlation between the step-size and neck lengths for myosins that had necks between 6.8 nm (2IQ-HMM) and 27.2 nm (8IQ-HMM). This strongly suggests that the step-size during a processive run is dictated primarily by the length of the neck and not solely by the pseudo-repeat of the actin filament. Thus, our study is consistent with and extends the previous study of Purcell et al. (*10*) where a 4IQ-HMM moved 24 nm and a 6IQ-HMM moved 36 nm in an optical trap under lightly loaded conditions. Our data, however, does not support the data of Tanaka et al. (*14*). It is possible that the step-size in the latter study was artifactually influenced by the nature of the construct which fused the motor domain and first IQ motif of myosin V with the rod region of smooth muscle myosin. Some studies suggest that the proximal rod region of smooth muscle myosin coiled-coil might only weakly dimerize and can possibly uncoil (*18*, *19*). However, Chakrabarty et al. (*20*) showed that this is not necessary for the two heads of smooth muscle myosin to bind simultaneously to actin.

Only one of the two heads of myosin was typically labeled in our assay. We observed the movement of the labeled trail head as it detached, was moved forward, and reattached as the new leading head. For the 6IQ-HMM, this movement corresponded to about 74 nm, but the center of mass of the molecule has only moved one-half of this distance (37 nm). Thus, the step-sizes measured in the FIONA assay are consistent with those measured by optical trapping where the center of mass movement of the bead is measured (*2*, *7*). In both the optical trapping studies where myosin V molecules were moving against load and in the FIONA system where there was no load, the step-size of 6IQ myosin V is matched with the helical repeat of the actin filament (*8*−*10*). In cells, this allows myosin V to move cargo along actin filaments that are attached to the cytoskeleton while keeping its load positioned above without the need to spiral around the helical actin filament.

The step-size distributions of the 2IQ-, 4IQ-, and 6IQ-HMM molecules were fit by a single Gaussian distribution. However, the data for 8IQ-HMM were more widely distributed with several distinct peaks and were best fit to the sum of five Gaussian functions, corresponding to three major peaks with step-sizes of 74, 93, and 110 nm and two small peaks of 133.5 and 165 nm. It is likely that the extra-long neck of the 8IQ-HMM allows the detached head to explore a larger area of the actin filament for binding sites. It is possible that the two small peaks with the greatest step-sizes represent instances where the myosin took three steps in rapid sequence with no obvious dwell period. The 74 nm peak could be explained if the two heads were initially separated by 37 nm (i.e., bound to the 0th and 13th actins in Figure 5a) with the trailing head detaching and rebinding at the 26th actin. This is the same distance and mechanism utilized by 6IQ-HMM. Similarly, the 110 nm movement could be explained if the two heads are initially 55 nm apart (corresponding to binding sites at the 0th and 20th actin positions) and where the trailing head detaches and reattaches 55 nm in front of the attached head at the 40th actin (Figure 5c). There are two possibilities to explain the 92 nm steps. If the two heads were initially bound at the 0th and 20th positions (55 nm apart) and the labeled trailing head detached and reattached at the 33rd position (the heads are now 37 nm apart), then a 92 nm step would occur (Figure 5b). Alternatively, the 92 nm step-size could be explained by a situation where the two heads are initially 37 nm apart (i.e., at the 0th and 13th positions) and upon taking the step the labeled head moves to the 42nd or 44th actin (55 nm in front of the attached head).

Both the 110 nm and the 92 nm step would require considerable azimuthal twisting of the myosin V heads as would the steps for 2IQ-HMM and 4IQ-HMM, implying that these molecules may spiral around the actin filament during processive runs (Figure 6). The expected degree of azimuthal tilting of the two heads are shown in Figure 6a for 4IQ-HMM (left), 6IQ-HMM (middle), and 8IQ-HMM (right). An overhead view delineating the position of the two heads of

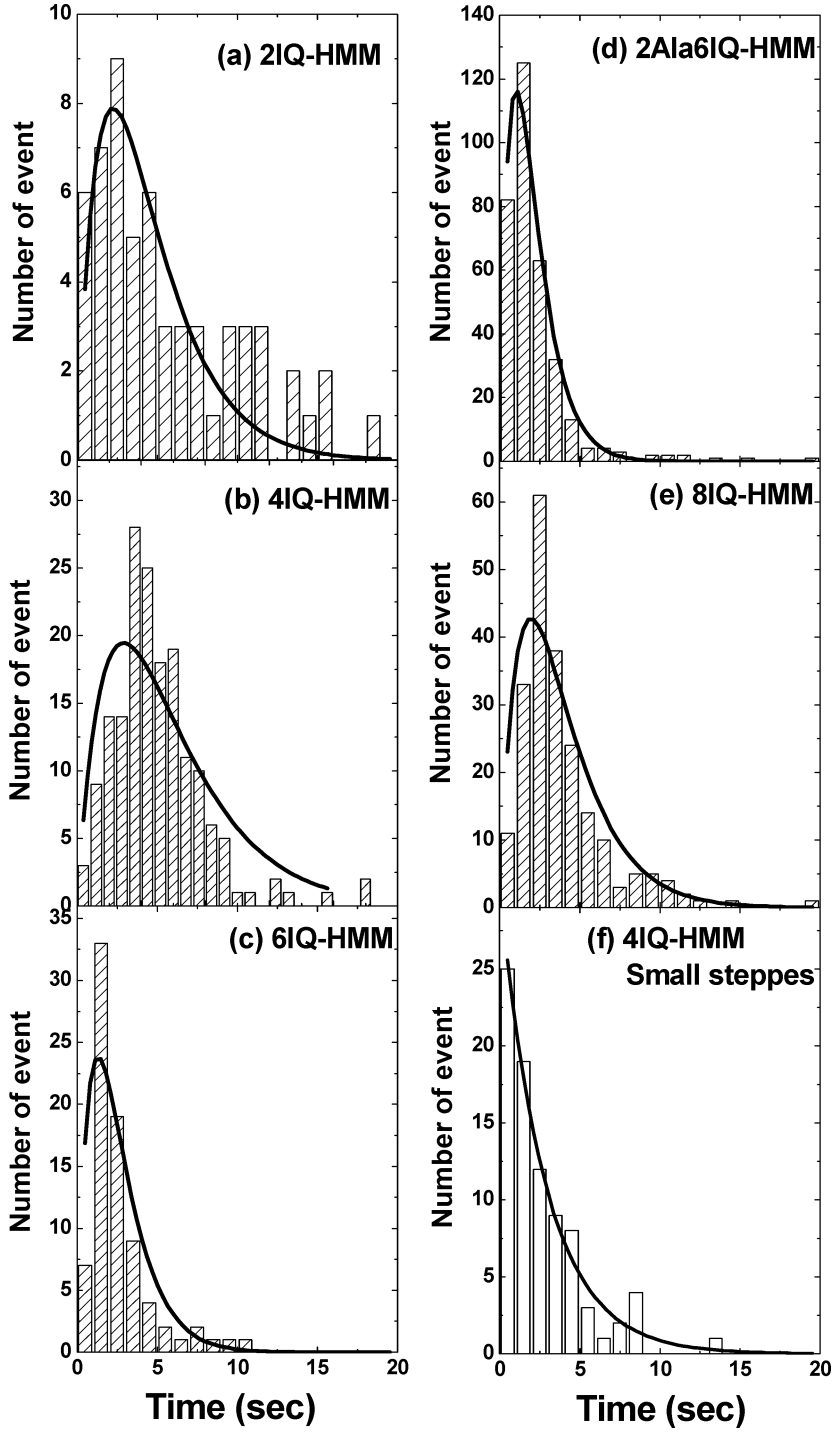

FIGURE 4: Histograms of dwell times of the large and small stepper traces of HMMM-IQ mutants. Dwell times for the large stepper traces of (a) 2IQ-HMM, (b) 4IQ-HMM, (c) 6IQ-HMM, (d) 2Als6IQ-HMM, and (e) 8IQ-HMM. Dwell time distributions for the small stepper traces of 4IQ-HMM (f). Histograms for the large steppers (a−e) were fit to an equation based on a hand-over-hand model equation; $F(t) = tk^2 \exp(-kt)$. The histogram for the small stepper trace (f) was fit to a single-exponential equation, $P(t) = k\, e^{-kt}$. The rate constants of the fits are 0.46 s^{-1} (2IQ-HMM), 0.28 s^{-1} (4IQ-HMM), 0.63 s^{-1} (6IQ-HMM), 0.82 s^{-1} (2Ala6IQ-HMM), and 0.4 s^{-1} (8IQ-HMM) for the large steppers and 0.47 s^{-1} for the 4IQ-HMM smaller steppers.

the same molecules is shown in Figure 6b. The diffusive search of the new leading head for a target actin monomer is shown in Figure 6c. Two positions of the attached post-power stroke lever-arm (at 30° and 50° with respect to the actin filament) are shown. Walker et al. (*21*) measured a 40° angle of the trailing head when both heads were attached, as seen by electron microscopy. Forkey et al. (*17*) using polarization techniques found that the angle varied between 0° and 50°. Thus, a diffusive search in which the attached post-power stroke lever-arm underwent as little as a 30−50° change in angle would allow the searching leading head to explore the appropriate landscape on actin.

Interestingly, the different HMM-IQ mutants gave different dwell times that did not correlate with the length of the neck in any predictable manner. The rate was fastest for 6IQ-HMM and about 2-fold slower for 4IQ-HMM. In optical

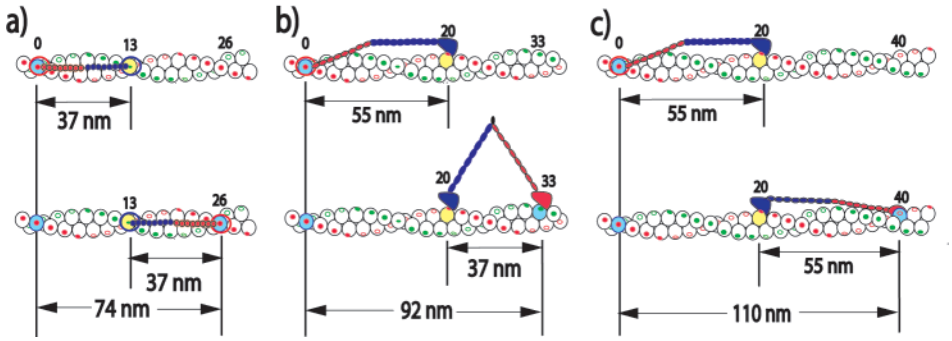

FIGURE 5: Three possible stepping pathways for 8IQ-HMM. The top panel shows the position of the two attached heads before the step occurs. The lower panel shows the position of the two heads after the step. The trailing head (red in upper panel) of the mutants starts out bound to actin no. 0. It detaches and moves forward to attach as the new leading head (lower panel). The numbers on or near the actin monomer describe its position relative to the actin monomer occupied by the initial trail head. (a) 8IQ-HMM undergoing a 74 nm step; (b) 8IQ-HMM taking a 92 nm step; (c) 8IQ-HMM taking a 110 nm step.

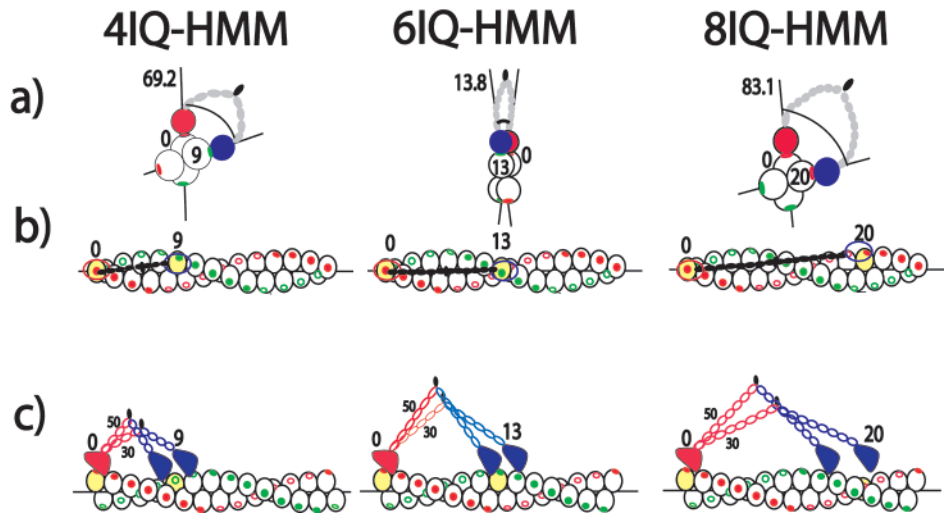

FIGURE 6: A model of the probability of new leading head reaching a particular binding site on actin. Binding geometries shown for the two heads of a 4IQ-HMM molecule (left), a 6IQ-HMM molecule (center), and an 8IQ-HMM molecule (right). In each case, the lead head is colored red and the trail head is blue. The top panel (a) is an end-on view down the length of an actin filament with an HMM bound via both heads. The black number inside or beside the actin monomers denotes the position along the filament that the two heads are bound (with the trailing head assigned a monomer position of 0). The number above the HMM gives the degree of azimuthal tilting the heads undergo when binding to the actin monomer numbered in the diagram. The middle panel (b) is a top view of the same HMM molecules bound to actin. The numbers inside or adjacent to the actin monomers give the position along the filament where the two heads are bound. The lower panel (c) is a side view of the same filament showing the diffusional search of the lead head for a suitable actin binding site. The large numbers above the actin monomers denote the position along the actin filament. The small numbers indicate that the lever-arm of the attached head is either at a 30° or 50° angle with respect to the actin filament as suggested by Walker et al. (*21*) and Forkey et al. (*17*).

trapping assays and TIRF single molecule movement assays, at limiting ATP concentrations, the rate of stepping of the 6IQ-HMM or intact myosin V molecules is consistent with the second-order rate constant of ATP binding to actomyosin V S1, as measured by transient kinetics (*2*, *7*). It is possible that the slower stepping mutants in this study have a slower rate of ATP binding due to distortion of the molecules caused by intramolecular strain as the two heads bind at different azimuthal angles. Thus, nature has designed the wild-type myosin V to be able to take multiple steps that coincide with the helical repeat of actin filaments. This allows the molecule to efficiently move on actin filaments that are firmly anchored to the cytoskeleton while keeping its cargo positioned above. The presence of strain-dependent intrahead gaiting of the product release rates from wild-type myosin V likely contributes to the processivity (*2*, *22*). The rate of movement of the 8IQ-HMM mutants in single-molecule TIRF assays at 2 mM ATP was slower than that of 6IQ-HMM despite the longer step-size in the former (*8*). This may reflect a loss of strain-dependent acceleration of the rate of ADP release from the trailing head in this mutant (*26*). If so, we provide further evidence that tampering with the wild-type neck alters the nucleotide binding and dissociation kinetics by disrupting the normal stereospecific attachment of myosin V to actin that has been finely tuned by nature.

NOTE ADDED AFTER PRINT PUBLICATION

The name of author Ahmet Yildiz was misspelled in the version published on the Web 11/16/05 (ASAP) and in the December 13, 2005, issue (Vol. 44, No. 49, pp 16203−16210). The correct electronic version was published 01/10/06, and an Addition and Correction appears in the February 7, 2006, issue (Vol. 45, No. 5).

ACKNOWLEDGMENT

We thank Dr. Earl Homsher, Mihaly Kovacs, and Yasuharu Takagi for helpful comments on the text and are

especially grateful to Estelle V. Harvey for expert technical assistance. We thank Dr. Douglas Ling for advice on the statistical analysis of the multimodal fits.

REFERENCES

1. De La Cruz, E. M., Wells, A. L., Rosenfeld, S. S., Ostap, E. M., and Sweeney, H. L. (1999) The kinetic mechanism of myosin V, *Proc. Natl. Acad. Sci. U.S.A. 96*, 13726−13731.
2. Mehta, A. D., Rock, R. S., Ridf, M., Spudich, J. A., Mooseker, M. S., and Cheney, R. E. (1999) Myosin-V is a processive actin-based motor, *Nature 400*, 590−593.
3. Sakamoto, T., Amitani, I., Yokota, E., and Ando, T. (2000) Direct observation of processive movement by individual myosin V molecules, *Biochem. Biophys. Res. Commun. 272*, 586−590.
4. Wu, X. S., Rao, K., Zhang, H., Wang, F., Sellers, J. R., Matesic, L. E., Copeland, N. G., Jenkins, N. A., and Hammer, J. A., III (2002) Identification of an organelle receptor for myosin-Va, *Nat. Cell Biol. 4*, 271−278.
5. Rogers, S. L., Karcher, R. L., Roland, J. T., Minin, A. A., Steffen, W., and Gelfand, V. I. (1999) Regulation of melanosome movement in the cell cycle by reversible association with myosin V, *J. Cell Biol. 146*, 1265−1276.
6. Cheney, R. E., O'Shea, M. K., Heuser, J. E., Coelho, M. V., Wolenski, J. S., Espreafico, E. M., Forscher, P., Larson, R. E., and Mooseker, M. S. (1993) Brain myosin-V is a two-headed unconventional myosin with motor activity, *Cell 75*, 13−23.
7. Veigel, C., Wang, F., Bartoo, M. L., Sellers, J. R., and Molloy, J. E. (2001) The gated gait of the precessive molecular motor, myosin V, *Nat. Cell Biol. 4*, 59−65.
8. Sakamoto, T., Wang, F., Schmitz, S., Xu, Y. H., Xu, Q., Molloy, J. E., Veigel, C., and Sellers, J. R. (2003) Neck length and processivity of myosin V, *J. Biol. Chem. 278*, 29201−29207.
9. Moore, J. R., Krementsova, E. B., Trybus, K. M., and Warshaw, D. M. (2004) Does the myosin V neck region act as a lever?, *J. Muscle Res. Cell Motil. 25*, 29−35.
10. Purcell, T. J., Morris, C., Spudich, J. A., and Sweeney, H. L. (2002) Role of the lever arm in the processive stepping of myosin V, *Proc. Natl. Acad. Sci. U.S.A. 99*, 14159−14164.
11. Warshaw, D. M., Guilford, W. H., Freyzon, Y., Krementsova, E., Palmiter, K. A., Tyska, M. J., Baker, J. E., and Trybus, K. M. (2000) The light chain binding domain of expressed smooth muscle heavy meromyosin acts as a mechanical lever, *J. Biol. Chem. 275*, 37167−37172.
12. Ruff, C., Furch, M., Brenner, B., Manstein, D. J., and Meyhofer, E. (2001) Single-molecule tracking of myosins with genetically engineered amplifier domains, *Nat. Struct. Biol. 8*, 226−229.
13. Warshaw, D. M. (2004) Lever arms and necks: a common mechanistic theme across the myosin superfamily, *J. Muscle Res. Cell Motil. 25*, 467−474.
14. Tanaka, H., Homma, K., Iwane, A. H., Katayama, E., Ikebe, R., Saito, J., Yanagida, T., and Ikebe, M. (2002) The motor domain determines the large step of myosin-V, *Nature 415*, 192−195.
15. Yildiz, A., Forkey, J. N., McKinney, S. A., Ha, T., Goldman, Y. E., and Selvin, P. R. (2003) Myosin V walks hand-over-hand: single fluorophore imaging with 1.5-nm localization, *Science 300*, 2061−2065.
16. Spudich, J. A., and Watt, S. (1971) The regulation of rabbit skeletal muscle contraction, *J. Biol. Chem. 246*, 4866−4871.
17. Forkey, J. N., Quinlan, M. E., Shaw, M. A., Corrie, J. E., and Goldman, Y. E. (2003) Three-dimensional structural dynamics of myosin V by single-molecule fluorescence polarization, *Nature 422*, 399−404.
18. Trybus, K. M., Freyzon, Y., Faust, L. Z., and Sweeney, H. L. (1997) Spare the rod, spoil the regulation: necessity for a myosin rod, *Proc. Natl. Acad. Sci. U.S.A. 94*, 48−52.
19. Sata, M., Matsuura, M., and Ikebe, M. (1996) Characterization of the motor and enzymatic properties of smooth muscle long SI and short HMM: role of the two-headed structure on the activity and regulation of the myosin motor, *Biochemistry 35*, 11113−11118.
20. Chakrabarty, T., Yengo, C., Baldacchino, C., Chen, L. Q., Sweeney, H. L., and Selvin, P. R. (2003) Does the S2 rod of myosin II uncoil upon two-headed binding to actin? A leucine-zippered HMM study, *Biochemistry 42*, 12886−12892.
21. Walker, M. L., Burgess, S. A., Sellers, J. R., Wang, F., Hammer, J. A., III, Trinick, J., and Knight, P. J. (2000) Two-headed binding of a processive myosin to F-actin, *Nature 405*, 804−807.
22. Rosenfeld, S. S., and Sweeney, H. L. (2004) A model of myosin V processivity, *J. Biol. Chem. 279*, 40100−40110.
23. Press, W. H., Flannery, B. P., and Teukolsky, S. A. (1992) *Numerical Recipes in Fortran 77*, Cambridge University Press, Cambridge, U.K.
24. Stratford, K. J., Jack, J. J., and Larkman, A. U. (1997) Calibration of an autocorrelation-based method for determining amplitude histogram reliability and quantal size, *J. Physiol. 505* (Pt. 2), 425−442.
25. Ling, D. S., and Benardo, L. S. (1999) Restrictions on inhibitory circuits contribute to limited recruitment of fast inhibition in rat neocortical pyramidal cells, *J. Neurophysiol. 82*, 1793−1807.
26. Veigel, C., Schmitz, S., Wang, F., and Sellers, J. R. (2005) Load-dependent kinetics of myosin-V can explain its high proessivity, *Nat. Cell Biol. 7*, 861−869.

BI0512086